AGU PUBLICATIONS

Geophysical Research Letters

RESEARCH LETTER

10.1002/2015GL063944

Key Points:
- Cross-shore exchange velocity due to transient rip currents is self-similar
- The exchange velocity profile is scaled by incident waves and beach slope
- Transient rip current exchange exceeds Stokes drift up to six surf zone widths

Correspondence to:
S. H. Suanda,
ssuanda@ucsd.edu

Citation:
Suanda, S. H., and F. Feddersen (2015), A self-similar scaling for cross-shelf exchange driven by transient rip currents, *Geophys. Res. Lett.*, *42*, 5427–5434, doi:10.1002/2015GL063944.

Received 23 MAR 2015
Accepted 16 JUN 2015
Accepted article online 18 JUN 2015
Published online 6 JUL 2015
Corrected 25 JAN 2016

This article was corrected on 25 JAN 2016. See the end of the full text for details.

A self-similar scaling for cross-shelf exchange driven by transient rip currents

Sutara H. Suanda[1] and Falk Feddersen[1]

[1] Scripps Institution of Oceanography, La Jolla, California, USA

Abstract Transient rip currents, episodic offshore flows from the surf zone to the inner shelf, present a recreational beach hazard and exchange material across the nearshore ocean. The magnitude and offshore extent of transient rip-current-induced exchange and its relative importance to other inner shelf exchange processes are poorly understood. Here 120 model simulations with random, normally incident, directionally spread waves spanning a range of beach slopes and wave conditions show that the transient rip current exchange velocity is self-similar. The nondimensional exchange velocity, surf zone flushing time, and cross-shore decay length scale are scaled by beach slope and wave properties, depending strongly on wave directional spread. Transient rip-current-driven exchange can be compared to other cross-shelf exchange processes. For example, transient rip-current-driven exchange is stronger than wave-induced Stokes-drift-driven exchange up to six surf zone widths from shore.

1. Introduction

The nearshore, the $\approx$ 1 km of ocean adjacent to the coastline, consists of the surf zone, where circulation is forced by breaking surface waves, and the inner shelf immediately offshore, where flows are driven by winds, buoyancy, tides, and nonbreaking waves [*Dalrymple et al.*, 2011; *Lentz and Fewings*, 2012]. Understanding cross-shelf exchange between the surf zone and inner shelf is challenging due to these dynamical differences yet essential to many areas of societal concern such as maintaining beaches, pollution dispersal, and managing coastal ecosystems. For example, tracers (e.g., terrestrial pollutants), introduced at the shoreline, are diluted in the surf zone by exchange with the inner shelf [e.g., *Hally-Rosendahl et al.*, 2014]. Additionally, the recruitment of intertidal invertebrate larvae depends on cross-shelf exchange processes [e.g., *Shanks and Wright*, 1987; *Fujimura et al.*, 2014].

A variety of physical processes can induce cross-shelf exchange. On the inner shelf, the vertical mismatch between offshore-directed undertow and onshore-wave-driven Stokes drift results in cross-shelf exchange [*Lentz et al.*, 2008; *Kirincich et al.*, 2009; *McPhee-Shaw et al.*, 2011]. At subtidal time scales, cross-shelf winds can induce cross-inner-shelf exchange particularly relative to along-shelf winds [*Fewings et al.*, 2008]. Shoreward propagating nonlinear internal waves [e.g., *Pineda*, 1991; *Sinnett and Feddersen*, 2014] and shelf eddies [e.g., *Romero et al.*, 2013; *Uchiyama et al.*, 2014] can also exchange material across the inner shelf.

Rip currents, concentrated, offshore-directed flows from the surf zone to the inner shelf, exchange sediments [*Shepard et al.*, 1941], pollutants [*Boehm et al.*, 2005], and larvae [*Shanks et al.*, 2010]. Rip currents are also a beach hazard accounting for 80% of U.S. lifeguard rescues, with more than 100 swimmer drownings each year [*MacMahan et al.*, 2006, 2010]. Rip currents are classified as bathymetrically controlled or transient. Bathymetrically controlled rip currents occur at fixed alongshore locations near structures or on embayed or rip-channeled beaches and can be considered part of the circulation [*MacMahan et al.*, 2010; *Dalrymple et al.*, 2011]. Modeling [*Reniers et al.*, 2010; *Castelle and Coco*, 2013] and observations [*MacMahan et al.*, 2010; *Brown et al.*, 2015] indicate that bathymetrically controlled rips can exchange material two to four surf zone widths from the shoreline.

In contrast, transient rip currents occur on alongshore uniform bathymetry and originate from surf zone eddies generated by finite-crest length wave breaking which then coalesce to larger scales [*Peregrine*, 1998; *Johnson and Pattiaratchi*, 2006; *Spydell and Feddersen*, 2009; *Clark et al.*, 2012]. Transient rip currents occur episodically for O (1 min), have short (10–100 m) alongshore length scales [*Hally-Rosendahl et al.*, 2014], and no preferred alongshore location [*Dalrymple et al.*, 2011] (Figure 1a). Thus, transient rip currents can be

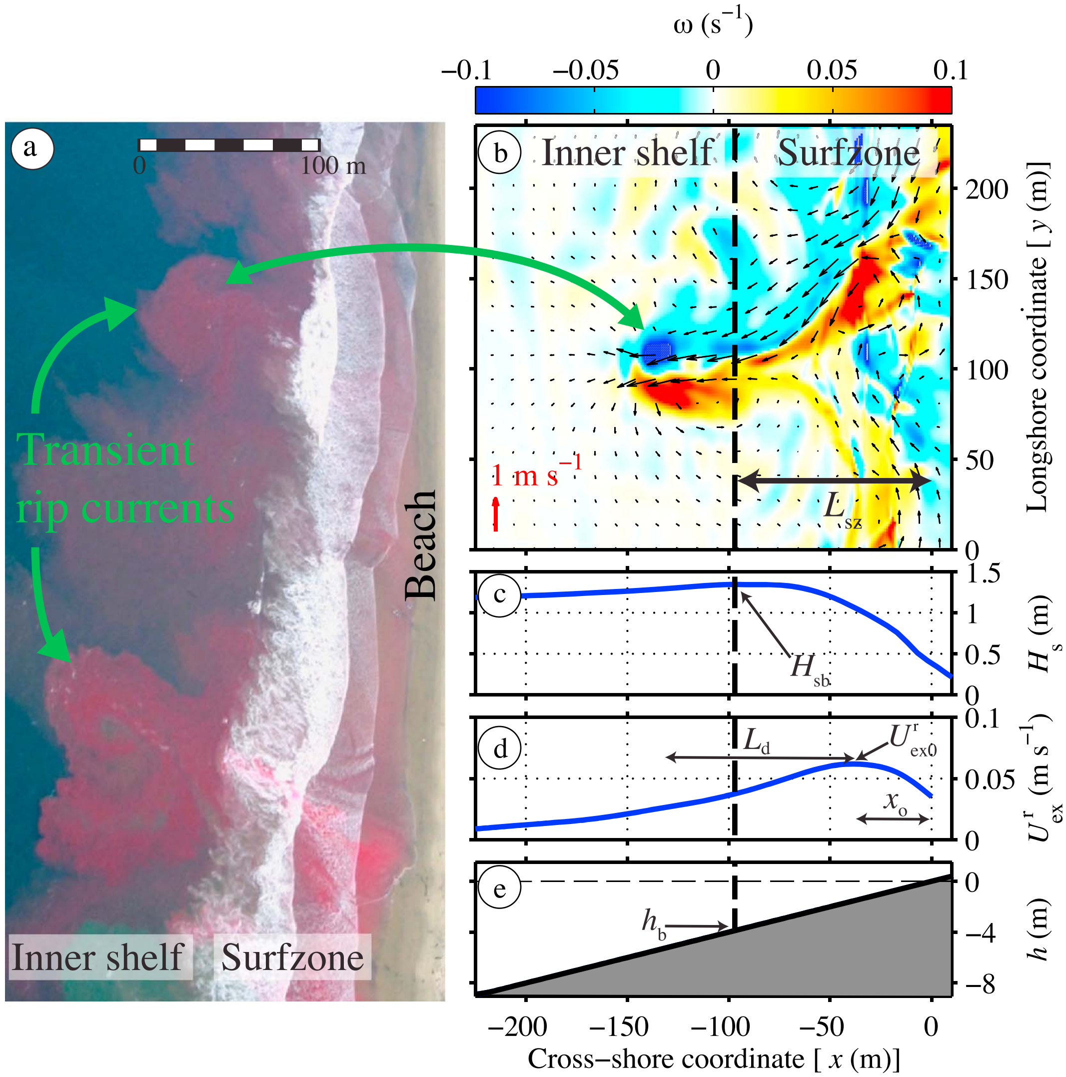

Figure 1. (a) Aerial photograph of an alongshore uniform beach during a shoreline dye release [*Hally-Rosendahl et al.*, 2014]. Dye is ejected from the surf zone to the inner shelf in plumes associated with transient rip currents. Results from a *funwaveC* simulation with $\beta = 0.04$ and incident $H_s = 1.1$ m, $T_p = 14$ s, $\sigma_\theta = 10°$: (b) Snapshot of vertical vorticity (ω) and current vectors for a subset of the model domain as a function of cross (x) and alongshore (y) coordinates for a well-developed transient rip current exiting the surf zone. (c) Significant wave height H_s, (d) time-mean transient rip-current-driven exchange velocity U^r_{ex}, and (e) planar bathymetry h versus x with shoreline at $x = 0$ m and the vertical dashed black line divides the surf zone and inner shelf ($x = L_{sz}$). The exchange velocity fit parameters (U^r_{ex0}, x_o, L_d) defined in (2) are noted in Figure 1d.

considered two-dimensional turbulence as their length scales are much longer than the water depth [*Feddersen*, 2014]. Although transient rip currents are ubiquitous on alongshore uniform beaches, few observational studies have attempted to quantify transient rip current exchange due to their episodic nature [*Johnson and Pattiaratchi*, 2004; *Hally-Rosendahl et al.*, 2014].

Previously, surf zone eddy intensity was shown to increase with wave directional spread σ_θ for the same significant wave height H_s and peak period T_p [*Spydell and Feddersen*, 2009]. As transient rip currents result from surf zone eddies, these wave parameters should also determine the exchange velocity from the surf zone to inner shelf representative of rip currents. Here cross-shelf exchange by transient rip currents is investigated with 120 simulations using a wave-resolving model *funwaveC*, spanning a range of normally incident wave conditions and beach slopes. The model setup and methods for estimating transient rip current exchange are presented (section 2). The cross-shore profile of transient rip current exchange is self-similar and is scaled by the incident wave conditions, particularly wave directional spread (section 3). The implications of transient rip currents on surf zone residence time and the relative importance of transient rip-current-driven exchange to wave-driven Stokes drift exchange on the inner shelf are discussed in section 4. The results are summarized in section 5.

2. Model and Methods

The wave-resolving model *funwaveC* [e.g., *Feddersen*, 2007; *Feddersen et al.*, 2011; *Guza and Feddersen*, 2012] solves the (vertically integrated) Boussinesq mass and momentum equations with nonlinear and dispersive effects [*Nwogu*, 1993] and parameterized wave breaking [*Kennedy et al.*, 2000]. The model has been shown to simulate well nearshore eddy variability and dye and drifter dispersion in comparison to field observations from multiple experiments on a range of beaches [*Spydell and Feddersen*, 2009; *Feddersen et al.*, 2011; *Clark et al.*, 2011; *Feddersen*, 2014]. In all simulations, the bathymetry is alongshore uniform (domain length, $L_y = 1200$ m), with an offshore flat region (depth, $h = 9$ m) where waves are generated and a planar slope region which extends above the mean water line allowing wave runup. A source function method [*Wei et al.*, 1999] generates normally incident random waves from a Pierson-Moskovitz spectrum [*Pierson and Moskowitz*, 1964], characterized by significant wave height H_s and peak period T_p. The normally incident waves have directional spread σ_θ [*Kuik et al.*, 1988] with a Gaussian shape that is uniform at all frequencies.

A total of 120 model simulations are performed spanning a range of beach slopes ($\beta = 0.02, 0.03, 0.04, 0.05$, and 0.06) and wave parameters significant wave height ($H_s = 0.5$, 0.8, and 1.1 m), peak period ($T_p = 8$ and 14 s), and wave directional spread ($\sigma_\theta = 2.5°, 5°, 10°$, and 20°). The peak period variation includes typical sea ($T_p = 8$ s) and swell ($T_p = 14$ s) cases. This dimensional parameter space yielded substantial variation in the relevant nondimensional parameters: deep-water wave steepness S_∞ and Irribarren number $\mathrm{Ir}_\infty = \beta/S_\infty$ (see section 3). Simulations were run for 8000 s, with the last 6000 s used for analysis once mean square vorticity has equilibrated [*Feddersen*, 2014]. Standard analyses [*Kuik et al.*, 1988] estimate $H_s(x)$ and bulk $\sigma_\theta(x)$.

Model horizontal velocities are decomposed into rotational (eddies and rip currents) and irrotational (wave) components [e.g., *Spydell and Feddersen*, 2009]. The net cross-shelf exchange due to transient rip currents is quantified using a rip current exchange velocity (U^r_{ex}), representative of the time- and alongshore-averaged exchange from the offshore-directed (negative) component of the rotational flow u^-_{rot}, i.e.,

$$U^r_{ex}(x) = \left\langle \frac{1}{L_y} \int u^-_{rot}(x, y, t)\mathrm{d}y \right\rangle, \tag{1}$$

where $\langle\rangle$ is a time average. The definition of U^r_{ex} (1) is analogous to the definition of estuarine total exchange flow [*MacCready*, 2011]. In calculating (1), the time mean of u_{rot} is removed to eliminate any potential standing rip current structures [i.e., *Johnson and Pattiaratchi*, 2006]. However, retaining the mean does not affect the results.

3. Results

An example simulation is shown in Figure 1. As random, normally incident, and directionally spread waves propagate over the bathymetry (h, Figure 1e), H_s increases to a maximum, defining the breakpoint location (Figure 1c), statistically delimiting the surf zone (of width $L_{sz} = 97$ m) and inner shelf [e.g., *Clark et al.*, 2010, 2011]. This L_{sz} definition gives similar results to that based on wave energy flux [e.g., *Spydell et al.*, 2009]. Quantities located at the breakpoint are denoted by subscript "b" (e.g., H_{sb}). Onshore of the breakpoint, H_s decays toward the shoreline as finite-crest length wave breaking generates vertical vorticity (eddies) [*Peregrine*, 1998; *Johnson and Pattiaratchi*, 2006; *Clark et al.*, 2012]. These eddies coalesce to larger scales [*Spydell and Feddersen*, 2009; *Feddersen*, 2014], resulting in episodic transient rip currents [*Johnson and Pattiaratchi*, 2006] with a vortex dipole signature and strong velocities, here > 1 m s^{-1} at $x = L_{sz}$ (Figure 1b). In this example, the maximum ($U_{ex0} = 0.06$ m s^{-1}) occurs at $x \approx L_{sz}/2$ (Figure 1d), decays as a Gaussian offshore, and remains significant (> 1 cm s^{-1}) up to 100 m beyond L_{sz}. As U^r_{ex} represents net exchange, it is far weaker than the $O(1)$ m s^{-1} maximum flow in an individual rip current (Figure 1b).

Similar to the example (Figure 1), over a range of β and wave conditions, $U^r_{ex}(x)$ profiles are approximately Gaussian with a maximum between 0.01–0.1 m s^{-1} and a cross-shore decay scale L_d of 50–250 m,

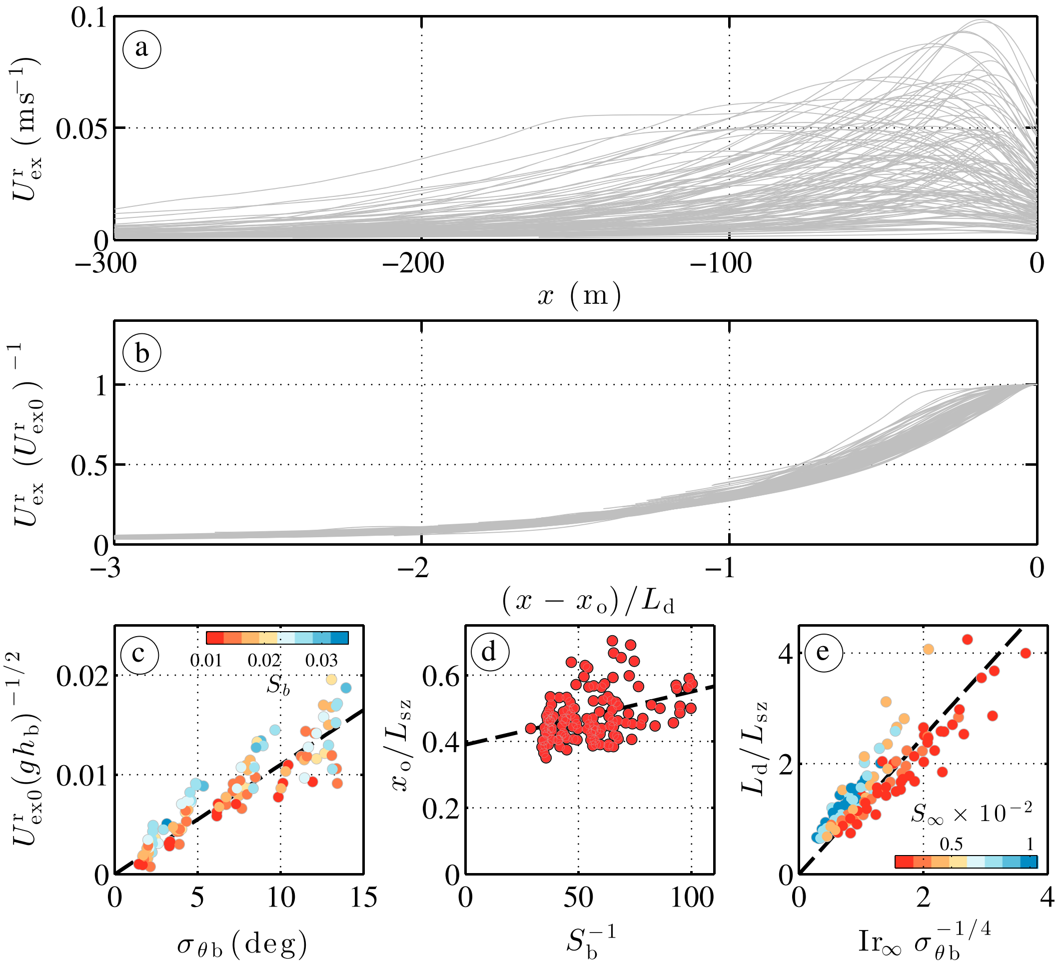

Figure 2. (a) Transient rip-current-driven exchange velocity U^{r}_{ex} versus cross-shore coordinate x for 120 model simulations. (b) Nondimensional U^{r}_{ex}/U^{r}_{ex0} versus nondimensional cross-shore coordinate $(x - x_o)/L_d$ using the exchange velocity fit parameters (U^{r}_{ex0}, x_o, L_d). Nondimensional dependencies for each fit parameter: (c) normalized maximum exchange velocity $U^{r}_{ex0}/(gh_b)^{1/2}$ versus breakpoint wave directional spread $\sigma_{\theta b}$ (in degrees) with breakpoint wave steepness S_b colored. (d) Location of maximum exchange velocity normalized by surf zone width x_o/L_{sz} versus inverse wave steepness S_b^{-1}, and (e) surf-zone-width-normalized cross-shore decay length scale L_d/L_{sz} versus $\mathrm{Ir}_\infty \sigma_{\theta b}^{-1/4}$ (where $\sigma_{\theta b}$ is in radians) with S_∞ colored.

comparable to the surf zone width L_{sz} (Figure 2a). The U^{r}_{ex} cross-shore profiles are well fit (regression skill > 0.8) to a Gaussian form,

$$U^{r}_{ex}(x) = U^{r}_{ex0} \exp\left[\frac{-(x - x_o)^2}{L_d^2}\right] \quad (2)$$

yielding three U^{r}_{ex} fit parameters (U^{r}_{ex0}, x_o, L_d) which are best fit using iterative least squares for each simulation. The nondimensionalized U^{r}_{ex}/U^{r}_{ex0} versus $(x - x_o)/L_d$ profiles collapse into a self-similar form (Figure 2b), suggesting a scaling law for transient rip-current-driven exchange velocity $U^{r}_{ex}(x)$.

The three exchange parameters (U^{r}_{ex0}, x_o, L_d) are nondimensionalized and scaled by the nondimensional wave parameters and beach slope β (Figures 2c–2e). Relevant nondimensional surf zone parameters are the wave steepness ($S = H_{s\infty}/L$, where $H_{s\infty}$ is the deep water H_s and L the local wavelength given from T_p and the wave phase speed) evaluated in deep water ($S_\infty = H_{s\infty}/L_\infty$) or at the breakpoint ($S_b = H_{s\infty}/L_b$), and deep-water Irribarren number [e.g., *Battjes*, 1974] $\mathrm{Ir}_{\infty,b} = \beta/S_{\infty,b}^{1/2}$. The maximum exchange velocity U^{r}_{ex0} is scaled by the breakpoint shallow water wave phase speed $(gh_b)^{1/2}$. The nondimensional $U^{r}_{ex0}(gh_b)^{-1/2}$ varies over a factor of 20 and depends strongly on the directional spread at the breakpoint $\sigma_{\theta b}$ with

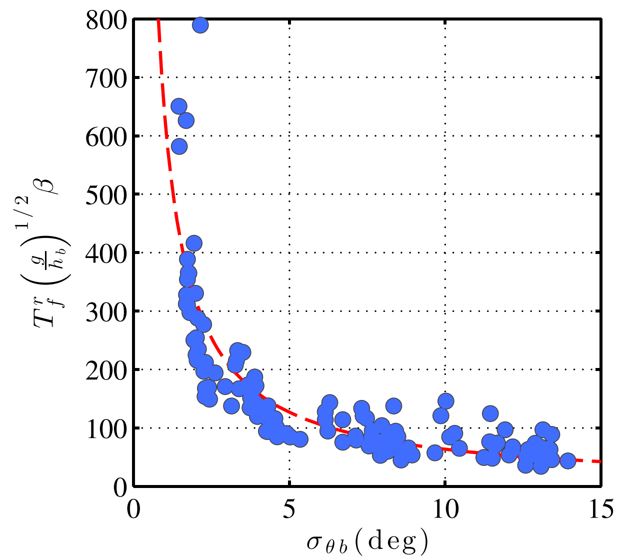

Figure 3. Nondimensional surf zone flushing time $T_f^r\,(g/h_\mathrm{b})^{1/2}\,\beta$ versus breakpoint wave directional spread $\sigma_{\theta\mathrm{b}}$ (in degrees). Red dashed curve shows $\sigma_{\theta\mathrm{b}}^{-1}$ dependence.

a weak dependence on S_b (Figure 2c). The strong $U^\mathrm{r}_\mathrm{ex0}$ dependence on wave directional spread $\sigma_{\theta\mathrm{b}}$ highlights the important role of finite-crest length wave breaking [*Peregrine*, 1998; *Clark et al.*, 2012] in generating surf zone vorticity that develops into transient rip currents. The nondimensional location of the maximum $x_\mathrm{o}/L_\mathrm{sz} \approx 0.5$ with small (± 0.1) variability and weak S_b^{-1} dependence (Figure 2d). The nondimensional cross-shore decay scale L_d/L_sz largely varies between 0.9 and 2.5. With $x_0/L_\mathrm{sz} \approx 0.5$, the U^r_ex *e*-folding decay location is 0.4–1.9 L_sz offshore of the surf zone to inner shelf boundary. The nondimensional L_d/L_sz is a strong function of $\mathrm{Ir}_\infty \sigma_{\theta\mathrm{b}}^{-1/4}$ with a subsequent weak S_∞ dependence (Figure 2e). Similar scaling results apply for root-mean-square rotational velocity. These nondimensional scalings are written as

$$\frac{U^\mathrm{r}_\mathrm{ex0}}{(gh_\mathrm{b})^{1/2}} = 2.9\times 10^{-2}\sigma_{\theta\mathrm{b}}\left[1+70S_\mathrm{b}\right], \quad \text{(3a)}$$

$$\frac{x_\mathrm{o}}{L_\mathrm{sz}} = 0.39\left[1+0.005S_\mathrm{b}^{-1}\right], \quad \text{(3b)}$$

$$\frac{L_\mathrm{d}}{L_\mathrm{sz}} = 0.58\mathrm{Ir}_\infty\sigma_{\theta\mathrm{b}}^{-1/4}\left[1+22S_\infty^{1/2}\right]. \quad \text{(3c)}$$

where $\sigma_{\theta\mathrm{b}}$ in (3) is given in radians. The $U^\mathrm{r}_\mathrm{ex0}(gh_b)^{-1/2}$ (3a) and $L_\mathrm{d}/L_\mathrm{sz}$ (3c) scalings have high squared correlation ($r^2 \geq 0.86$), indicating that they can accurately reproduce the dimensional exchange parameters. The $x_\mathrm{o}/L_\mathrm{sz}$ (3b) scaling has low $r^2 = 0.05$; however, the weak $x_\mathrm{o}/L_\mathrm{sz}$ variability indicates that simply using the mean value $\langle x_\mathrm{o}/L_\mathrm{sz}\rangle = 0.48$ is largely appropriate.

Using the scalings (equations (3a)–(3c)), the three scaled U^r_ex parameters (denoted with a tilde; $\tilde{U}^\mathrm{r}_\mathrm{ex0}$, $\tilde{x}_\mathrm{o}$, and $\tilde{L}_\mathrm{d}$) can be estimated from the wave parameters and β directly. Though more scattered than the nondimensional profiles (Figure 2b), the scaled profiles $U^\mathrm{r}_\mathrm{ex}/\tilde{U}^\mathrm{r}_\mathrm{ex0}$ versus $(x-\tilde{x}_\mathrm{o})/\tilde{L}_\mathrm{d}$ also largely collapse with small standard deviation relative to the mean (< 15%, not shown). All wave parameters (H_s, T_p, and σ_θ) can be predicted with modern spectral wave models, and the scaling laws can be used to estimate cross-shelf transient rip current exchange.

4. Discussion

Analogous to estuarine flushing time [*MacCready*, 2011; *Lemagie and Lerczak*, 2014], a bulk surf zone flushing time is useful in understanding surf zone to inner shelf material exchange. Here the transient rip current surf zone flushing time T_f^r is defined as the time required to replace the surf zone area ($A_\mathrm{sz} = h_\mathrm{b}L_\mathrm{sz}/2$),

$$T_f^r = \frac{A_\mathrm{sz}}{h_\mathrm{b}U^\mathrm{r}_\mathrm{ex}(L_\mathrm{sz})} = \frac{1}{2}\frac{L_\mathrm{sz}}{U^\mathrm{r}_\mathrm{ex}(L_\mathrm{sz})}. \quad (4)$$

where U^r_ex is evaluated at the surf zone inner shelf boundary ($x = L_\mathrm{sz}$). Short flushing times represent more rapid exchange of material. For all simulations, the dimensional T_f^r generally varies between 20 min and 3 h. Based on the U^r_ex scalings (equations (3a)–(3c)), the nondimensional flushing time $T_f^r(g/h_\mathrm{b})^{1/2}\beta$ varies more than an order of magnitude and depends proportionally on σ_θ^{-1} (Figure 3). The dimensional surf zone flushing time $T_f^r \propto (h_b/g)^{1/2}(\beta\sigma_{\theta\mathrm{b}})^{-1}$ is thus larger for deeper breakpoint depths h_b, shallower surf zone slopes, and smaller directional spreads. With $\sigma_{\theta\mathrm{b}} = 0°$, no transient rip currents are generated and T_f^r is infinite.

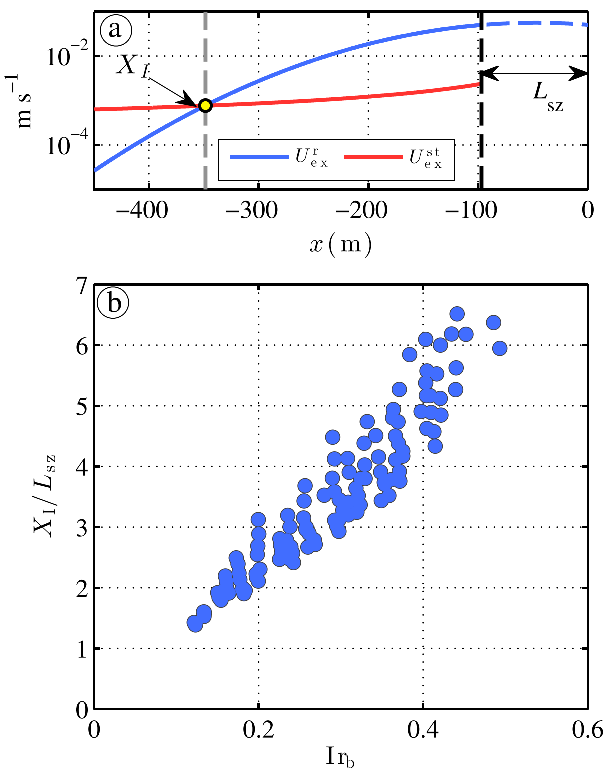

Figure 4. (a) Transient rip current (U^{r}_{ex}, blue) and Stokes drift (U^{st}_{ex}, red) exchange velocities versus x for the simulation shown in Figure 1. Note the logarithmic vertical axis. The location ($X_I = 353$ m) where $U^{r}_{ex} = U^{st}_{ex}$ (yellow circle, gray line) is 3.5 times the surf zone width ($L_{sz} = 97$ m, black dashed line). (b) Nondimensional intersection location X_I/L_{sz} versus breakpoint Irribarren number $\mathrm{Ir_b} = \beta/S_b^{1/2}$ for all simulations. A value of $X_I/L_{sz} = 2$ indicates that transient rip-current-driven exchange is greater than Stokes-drift-driven exchange up to two surf zone widths from the shoreline.

Transient rip-current-driven exchange is also estimated by advecting randomly seeded surf zone particles. The *e*-folding time for particles to leave the surf zone also yields a flushing time and, with (4), an exchange velocity. This velocity is well correlated with $U^{r}_{ex}(L_{sz})$ ($r^2 = 0.76$) with a regression slope of 5 due to particle recirculation typically accounted for by an exchange factor [*Lemagie and Lerczak*, 2014]. Thus, $U^{r}_{ex}(L_{sz})$ is representative of the surf zone flushing rate and the scalings (3) allow the surf zone flushing time to be quantified via (4).

On alongshore uniform coasts, wave-driven exchange across the inner shelf is usually attributed to the imbalance between vertical profiles of onshore wave-driven Stokes drift transport and offshore-directed Eulerian return flow [*Monismith and Fong*, 2004; *Lentz et al.*, 2008; *Lentz and Fewings*, 2012], defining a Stokes exchange velocity U^{st}_{ex}. The depth-integrated model *funwaveC* does not resolve the vertical structure of velocity. Instead, as inner shelf Eulerian return flow (undertow) is observed to be largely depth uniform with weak vertical shear [*Faria et al.*, 2000], Stokes-drift-induced exchange velocity $U^{st}_{ex}(x)$ are estimated assuming onshore Stokes drift balanced by a depth-uniform offshore flow [*Hally-Rosendahl et al.*, 2014],

$$U^{st}_{ex} = \frac{1}{8}(H_s k_p)^2 \frac{c}{\sinh^2(k_p h)} \left[\frac{1}{h} \int_{z_c}^{0} \left(\cosh(2k_p(z+h)) - \frac{\sinh(2k_p h)}{2k_p h} \right) \mathrm{d}z \right], \tag{5}$$

where k_p is the peak wave number, c is the linear phase speed, and the integral is from the integrand zero crossing (z_c) to the surface. Note, this U^{st}_{ex} (5) will be an overestimate if offshore Eulerian return flow is surface intensified [*Putrevu and Svendsen*, 1993; *Lentz et al.*, 2008].

Previously, inner shelf drifter velocities near the surf zone have been attributed to Stokes drift [*Ohlmann et al.*, 2012]. Here transient rip current (U^{r}_{ex}) and Stokes-drift-driven (U^{st}_{ex}) exchange velocities are compared to determine the offshore extent of transient rip current importance relative to Stokes drift. For the simulation shown in Figure 1, at the breakpoint ($L_{sz} = 97$ m), $U^{r}_{ex} \approx 0.04$ m s^{-1}, much larger than $U^{st}_{ex} \approx 0.002$ m s^{-1}. Farther offshore U^{r}_{ex} decays more rapidly than U^{st}_{ex} where they become equivalent at $X_I = 353$ m with magnitude 8×10^{-4} m s^{-1} (Figure 4a). The nondimensional location (relative to the shoreline) where $U^{r}_{ex} = U^{st}_{ex}$ (defined as X_I/L_{sz}) generally varies from two to six and is linearly scaled with the breaking Irribarren number $\mathrm{Ir_b} = \beta/S_b^{1/2}$ (Figure 4b). This indicates that transient rip-current-driven exchange is larger than the Stokes exchange up to two to six surf zone widths from shore well onto the inner shelf, in regions previously not thought to be influenced by the surf zone.

5. Summary

The wave-resolving model *funwaveC*, was used to simulate the cross-shore exchange induced by transient rip currents for a variety of normally incident, directionally spread random waves and beach slopes. The cross-shore profile of transient rip current exchange velocity is self-similar whose maximum magnitude, peak location, and cross-shore decay length scale is accurately scaled by the beach slope and incident wave conditions. The wave directional spread strongly influences the exchange velocity due to its role in surf zone vorticity generation. The transient rip current exchange velocity cross-shore decay length scale is up to 2.5 times the surf zone width, indicating the importance of surf zone processes on the inner shelf. These scalings can be used to quantify the surf zone flushing time which also depends on wave directional spread. These scaling laws allow estimation of the transient rip current cross-shelf exchange velocity and comparison to other inner shelf exchange processes such as shoaling internal waves, shelf eddies, or wind-driven circulation. For example, transient rip current exchange velocity can be stronger than wave-induced Stokes drift exchange velocity up to six surf zone widths from shore well onto the inner shelf.

Acknowledgments

Support was provided by the National Science Foundation (NSF) and the Office of Naval Research (ONR). We thank N. Kumar, M. S. Spydell, M. H. Martinez, and R. T. Guza for helpful discussions on the manuscript. The numerical model, *funwaveC*, is available online at http://iod.ucsd.edu/~falk/funwaveC.html. Results from simulations used in this work are available through the corresponding author in accordance with AGU data policy.

The Editor thanks two anonymous reviewers for their assistance in evaluating this paper.

References

Battjes, J. A. (1974), Surf similarity, in *Proceedings of the 14th Coastal Engineering Conference, Copenhagen, Denmark*, pp. 466–480, Am. Soc. Civ. Eng., New York., doi:10.9753/icce.v14, 24–28 June.

Boehm, A. B., D. P. Keymer, and G. G. Shellenbarger (2005), An analytical model of enterococci inactivation, grazing, and transport in the surf zone of a marine beach, *Water Res.*, *39*(15), 3565–3578.

Brown, J. A., J. H. MacMahan, A. J. H. M. Reniers, and E. B. Thornton (2015), Field observations of surf zone-inner shelf exchange on a rip-channeled beach, *J. Phys. Oceanogr.*, doi:10.1175/JPO-D-14-0118.1, in press.

Castelle, B., and G. Coco (2013), Surf zone flushing on embayed beaches, *Geophys. Res. Lett.*, *40*, 2206–2210, doi:10.1002/grl.50485.

Clark, D. B., F. Feddersen, and R. T. Guza (2010), Cross-shore surfzone tracer dispersion in an alongshore current, *J. Geophys. Res.*, *115*, C10035, doi:10.1029/2009JC005683.

Clark, D. B., F. Feddersen, and R. T. Guza (2011), Modeling surf zone tracer plumes: 2. Transport and dispersion, *J. Geophys. Res.*, *116*, C11028, doi:10.1029/2011JC007211.

Clark, D. B., S. Elgar, and B. Raubenheimer (2012), Vorticity generation by short-crested wave breaking, *Geophys. Res. Lett.*, *39*, L24604, doi:10.1029/2012GL054034.

Dalrymple, R. A., J. H. MacMahan, A. J. Reniers, and V. Nelko (2011), Rip currents, *Annu. Rev. Fluid Mech.*, *43*(1), 551–581, doi:10.1146/annurev-fluid-122109-160733.

Faria, A. F. G., E. B. Thornton, T. C. Lippmann, and T. P. Stanton (2000), Undertow over a barred beach, *J. Geophys. Res.*, *105*(C7), 16,999–17,010, doi:10.1029/2000JC900084.

Feddersen, F. (2007), Breaking wave induced cross-shore tracer dispersion in the surfzone: Model results and scalings, *J. Geophys. Res.*, *112*, C09012, doi:10.1029/2006JC004006.

Feddersen, F. (2014), The generation of surfzone eddies in a strong alongshore current, *J. Phys. Oceanogr.*, *44*(2), 600–617, doi:10.1175/JPO-D-13-051.1.

Feddersen, F., D. B. Clark, and R. T. Guza (2011), Modeling surf zone tracer plumes: 1. Waves, mean currents, and low-frequency eddies, *J. Geophys. Res.*, *116*, C11027, doi:10.1029/2011JC007210.

Fewings, M., S. J. Lentz, and J. Fredericks (2008), Observations of cross-shelf flow driven by cross-shelf winds on the inner continental shelf, *J. Phys. Oceanogr.*, *38*(11), 2358–2378, doi:10.1175/2008JPO3990.1.

Fujimura, A. G., A. J. H. M. Reniers, C. B. Paris, A. L. Shanks, J. H. MacMahan, and S. G. Morgan (2014), Numerical simulations of larval transport into a rip-channeled surf zone, *Limnol. Oceanogr.*, *59*(4), 1434–1447, doi:10.4319/lo.2014.59.4.1434.

Guza, R. T., and F. Feddersen (2012), Effect of wave frequency and directional spread on shoreline runup, *Geophys. Res. Lett.*, *39*, L11607, doi:10.1029/2012GL051959.

Hally-Rosendahl, K., F. Feddersen, and R. T. Guza (2014), Cross-shore tracer exchange between the surfzone and inner-shelf, *J. Geophys. Res. Oceans*, *119*, 4367–4388, doi:10.1002/2013JC009722.

Johnson, D., and C. Pattiaratchi (2004), Transient rip currents and nearshore circulation on a swell-dominated beach, *J. Geophys. Res.*, *109*, C02026, doi:10.1029/2003JC001798.

Johnson, D., and C. Pattiaratchi (2006), Boussinesq modelling of transient rip currents, *Coastal Eng.*, *53*(5–6), 419–439, doi:10.1016/j.coastaleng.2005.11.005.

Kennedy, A., Q. Chen, J. Kirby, and R. Dalrymple (2000), Boussinesq modeling of wave transformation, breaking, and runup. I: 1D, *J. Waterw. Port Coastal Ocean Eng.*, *126*(1), 39–47, doi:10.1061/(ASCE)0733-950X(2000)126:1(39).

Kirincich, A. R., S. J. Lentz, and J. A. Barth (2009), Wave-driven inner-shelf motions on the Oregon coast, *J. Phys. Oceanogr.*, *39*, 2942–2956.

Kuik, A. J., G. P. Van Vledder, and L. H. Holthuijsen (1988), A method for the routine analysis of pitch-and-roll buoy wave data, *J. Phys. Oceanogr.*, *18*(7), 1020–1034.

Lemagie, E. P., and J. A. Lerczak (2014), A comparison of bulk estuarine turnover timescales to particle tracking timescales using a model of the Yaquina Bay Estuary, *Estuaries Coasts*, 1–18, doi:10.1007/s12237-014-9915-1.

Lentz, S. J., and M. R. Fewings (2012), The wind-and wave-driven inner-shelf circulation, *Annu. Rev. Mar. Sci.*, *4*, 317–343.

Lentz, S. J., M. Fewings, P. Howd, J. Fredericks, and K. Hathaway (2008), Observations and a model of undertow over the inner continental shelf, *J. Phys. Oceanogr.*, *38*, 2341–2357.

MacCready, P. (2011), Calculating estuarine exchange flow using isohaline coordinates, *J. Phys. Oceanogr.*, *41*(6), 1116–1124, doi:10.1175/2011JPO4517.1.

MacMahan, J., et al. (2010), Mean Lagrangian flow behavior on an open coast rip-channeled beach: A new perspective, *Mar. Geol.*, *268*(1–4), 1–15, doi:10.1016/j.margeo.2009.09.011.

MacMahan, J. H., E. B. Thornton, and A. J. H. M. Reniers (2006), Rip current review, *Coastal Eng.*, *53*(2–3), 191–208, doi:10.1016/j.coastaleng.2005.10.009.

McPhee-Shaw, E. E., K. J. Nielsen, J. L. Largier, and B. A. Menge (2011), Nearshore chlorophyll-a events and wave-driven transport, *Geophys. Res. Lett.*, *38*, L02604, doi:10.1029/2010GL045810.

Monismith, S. G., and D. A. Fong (2004), A note on the potential transport of scalars and organisms by surface waves, *Limnol. Oceanogr.*, *49*(4), 1214–1217.

Nwogu, O. (1993), Alternative form of Boussinesq equations for nearshore wave propagation, *J. Waterw. Port Coastal Ocean Eng.*, *119*(6), 618–638, doi:10.1061/(ASCE)0733-950X(1993)119:6(618).

Ohlmann, J. C., M. R. Fewings, and C. Melton (2012), Lagrangian observations of inner-shelf motions in Southern California: Can surface waves decelerate shoreward-moving drifters just outside the surf zone?, *J. Phys. Oceanogr.*, *42*(8), 1313–1326, doi:10.1175/JPO-D-11-0142.1.

Peregrine, D. H. (1998), Surf zone currents, *Theor. Comput. Fluid Dyn.*, *10*(1–4), 295–309.

Pierson, W. J., and L. Moskowitz (1964), A proposed spectral form for fully developed wind seas based on the similarity theory of S. A. Kitaigorodskii, *J. Geophys. Res.*, *69*(24), 5181–5190, doi:10.1029/JZ069i024p05181.

Pineda, J. (1991), Predictable upwelling and the shoreward transport of planktonic larvae by internal tidal bores, *Science*, *253*(5019), 548–549, doi:10.1126/science.253.5019.548.

Putrevu, U., and I. A. Svendsen (1993), Vertical structure of the undertow outside the surf zone, *J. Geophys. Res.*, *98*(C12), 22,707–22,716, doi:10.1029/93JC02399.

Reniers, A. J., J. H. MacMahan, F. J. Beron-Vera, and M. J. Olascoaga (2010), Rip-current pulses tied to Lagrangian coherent structures, *Geophys. Res. Lett.*, *37*, L05605, doi:10.1029/2009GL041443.

Romero, L., Y. Uchiyama, J. C. Ohlmann, J. C. McWilliams, and D. A. Siegel (2013), Simulations of nearshore particle-pair dispersion in Southern California, *J. Phys. Oceanogr.*, *43*(9), 1862–1879, doi:10.1175/JPO-D-13-011.1.

Shanks, A. L., and W. G. Wright (1987), Internal-wave-mediated shoreward transport of cyprids, megalopae, and gammarids and correlated longshore differences in the settling rate of intertidal barnacles, *J. Exp. Mar. Biol. Ecol.*, *114*(1), 1–13.

Shanks, A. L., S. G. Morgan, J. MacMahan, and A. J. Reniers (2010), Surf zone physical and morphological regime as determinants of temporal and spatial variation in larval recruitment, *J. Exp. Mar. Biol. Ecol.*, *392*(1–2), 140–150, doi:10.1016/j.jembe.2010.04.018.

Shepard, F. P., K. O. Emery, and E. C. La Fond (1941), Rip currents: A process of geological importance, *J. Geol.*, *49*(4), 337–369, doi:10.1086/624971.

Sinnett, G., and F. Feddersen (2014), The surf zone heat budget: The effect of wave breaking, *Geophys. Res. Lett.*, *41*, 7217–7226, doi:10.1002/2014GL061398.

Spydell, M., and F. Feddersen (2009), Lagrangian drifter dispersion in the surf zone: Directionally spread, normally incident waves, *J. Phys. Oceanogr.*, *39*(4), 809–830.

Spydell, M. S., F. Feddersen, and R. T. Guza (2009), Observations of drifter dispersion in the surfzone: The effect of sheared alongshore currents, *J. Geophys. Res.*, *114*, C07028, doi:10.1029/2009JC005328.

Uchiyama, Y., E. Y. Idica, J. C. McWilliams, and K. D. Stolzenbach (2014), Wastewater effluent dispersal in Southern California bays, *Cont. Shelf Res.*, *76*, 36–52, doi:10.1016/j.csr.2014.01.002.

Wei, G., J. T. Kirby, and A. Sinha (1999), Generation of waves in Boussinesq models using a source function method, *Coastal Eng.*, *36*(4), 271–299, doi:10.1016/S0378-3839(99)00009-5.

Errattum

In the originally published version of this article, there were errors in equation 3a and equation 3c due to a conversion error from degrees to radians. Equations 3a and 3c have since been corrected, and this version may be considered the authoritative version of record. In equation 3a, “8.7×10^{-6}” has been changed to “2.9×10^{-2}”, and in equation 3c, "4.37Ir" has been changed to "0.58Ir".